THE JOURNAL OF BIOLOGICAL CHEMISTRY VOL. 283, NO. 18, pp. 12093–12101, May 2, 2008

Ablation of Ca^{2+} Channel β3 Subunit Leads to Enhanced *N*-Methyl-D-aspartate Receptor-dependent Long Term Potentiation and Improved Long Term Memory*[S]

Received for publication, January 31, 2008, and in revised form, March 12, 2008 Published, JBC Papers in Press, March 13, 2008, DOI 10.1074/jbc.M800816200

Daejong Jeon[‡§], Inseon Song[‡], William Guido[¶], Karam Kim[‖], Eunjoon Kim[‖], Uhtaek Oh[§1], and Hee-Sup Shin[‡2]

From the [‡]Center for Neural Science, Korea Institute of Science and Technology, Seoul 136-791, Korea, [§]National Creative Research Initiative Center for Sensory Research, Seoul National University, College of Pharmacy, Seoul 151-742, Korea, the [¶]Department of Anatomy and Neurobiology, Virginia Commonwealth University Medical Center, Richmond, Virginia 23298, and [‖]National Creative Research Initiative Center for Synaptogenesis, Department of Biological Sciences, Korea Advanced Institute of Science and Technology, Daejeon 305-701, Korea

The β subunits of voltage-dependent Ca^{2+} channels (VDCCs) have marked effects on the properties of the pore-forming α_1 subunits of VDCCs, including surface expression of channel complexes and modification of voltage-dependent kinetics. Among the four different β subunits, the β_3 subunit ($Ca_v\beta3$) is abundantly expressed in the hippocampus. However, the role of $Ca_v\beta3$ in hippocampal physiology and function *in vivo* has never been examined. Here, we investigated $Ca_v\beta3$-deficient mice for hippocampus-dependent learning and memory and synaptic plasticity at hippocampal CA3-CA1 synapses. Interestingly, the mutant mice exhibited enhanced performance in several hippocampus-dependent learning and memory tasks. However, electrophysiological studies revealed no alteration in the Ca^{2+} current density, the frequency and amplitude of miniature excitatory postsynaptic currents, and the basal synaptic transmission in the mutant hippocampus. On the other hand, however, *N*-methyl-D-aspartate receptor (NMDAR)-mediated synaptic currents and NMDAR-dependent long term potentiation were significantly increased in the mutant. Protein blot analysis showed a slight increase in the level of NMDAR-2B in the mutant hippocampus. Our results suggest a possibility that, unrelated to VDCCs regulation, $Ca_v\beta3$ negatively regulates the NMDAR activity in the hippocampus and thus activity-dependent synaptic plasticity and cognitive behaviors in the mouse.

Voltage-dependent Ca^{2+} channels (VDCCs)[3] play important roles in the regulation of diverse neuronal functions by mediating Ca^{2+} entry into cells. VDCCs have multiple subunit structures consisting of a major pore-forming subunit (α_1) and several auxiliary subunits ($\alpha_2\delta$, β, and γ) (1, 2). VDCCs are classified into L-type ($Ca_v1.1$, $Ca_v1.2$, $Ca_v1.3$, and $Ca_v1.4$: α_1S, α_1C, α_1D, and α_1F, respectively), P/Q-type ($Ca_v2.1$: α_1A), N-type ($Ca_v2.2$: α_1B), R-type ($Ca_v2.3$: α_1E), and T-type ($Ca_v3.1$, $Ca_v3.2$, and $Ca_v3.3$: α_1G, α_1H, and α_1I, respectively) based on electrophysiological and pharmacological properties (3). Among the auxiliary subunits, the β subunits are entirely cytosolic, and they have marked effects on the properties of VDCCs α_1 subunits, including trafficking of Ca^{2+} channel complexes to the plasma membrane, voltage dependence and activation/inactivation kinetics of Ca^{2+} currents (4, 5). Four β subunits ($Ca_v\beta1$–4) have been cloned, and each $Ca_v\beta$ has distinctive properties (5), but their functional roles in the brain *in vivo* are still poorly understood.

Structurally, $Ca_v\beta$ has five different domains, with the two conserved domains sharing significant homology among the β subunits. The conserved domains were revealed as an Src homology 3 (SH3) domain and a guanylate kinase (GK) domain (6–9), and thus $Ca_v\beta$ is included in membrane-associated guanylate kinase family that has scaffolding functions. Interestingly, it has been suggested that $Ca_v\beta$ can bind to other molecules (10, 11). For example, $Ca_v\beta$ could directly interact with small G-proteins (Gem and Rem) and dynamin (12–14). In addition, recent studies have suggested that $Ca_v\beta$ can work without marked influence on VDCCs. For example, regulation of gene transcription by a direct interaction between a short splice variant of $Ca_v\beta4$ and a nuclear protein was shown in the cochlea (15). $Ca_v\beta3$ was also shown to regulate insulin secretion by acting on the intracellular Ca^{2+} store, whereas Ca^{2+} currents of VDCCs were not affected (16). This study suggests that $Ca_v\beta$ can function as a multifunctional protein.

Of the $Ca_v\beta$ subunits, $Ca_v\beta3$ is highly expressed in the brain, especially in the hippocampus (17). It was shown that α_1 subunits of N- and L-type VDCCs were preferentially associated

* This work was supported by the National Honor Scientist Program of Korea, grants from Korea Institute of Science and Technology, the National Creative Research Initiatives of the Ministry of Science and Technology of Korea, and Virginia Commonwealth University Medical Center Grant NEI EY12716. The costs of publication of this article were defrayed in part by the payment of page charges. This article must therefore be hereby marked "*advertisement*" in accordance with 18 U.S.C. Section 1734 solely to indicate this fact.

[S] The on-line version of this article (available at http://www.jbc.org) contains supplemental Figs. S1 and S2.

[1] To whom correspondence may be addressed. Tel.: 82-2-880-7854; Fax: 82-2-872-0596; E-mail: utoh@plaza.snu.ac.kr.

[2] To whom correspondence may be addressed. Tel.: 82-2-958-6931; Fax: 82-2-958-6937; E-mail: shin@kist.re.kr.

[3] The abbreviations used are: VDCC, voltage-dependent Ca^{2+} channel; $Ca_v\beta3$, Ca^{2+} channels β_3 subunit; EPSC, excitatory postsynaptic current; mEPSCs, miniature EPSC; LTP, long term potentiation; NMDAR, *N*-methyl-D-aspartate receptor; AMPA, α-amino-3-hydroxy-5-methyl-4-isoxazolepropionic acid; AMPAR, AMPA receptor; CS, conditioned stimulus; GAD, glutamate decarboxylase; AHP, after hyperpolarization; fEPSPs, field excitatory postsynaptic potentials; SH3, Src homology 3; GK, guanylate kinase; ANOVA, analysis of variance; GABA, γ-aminobutyric acid; PPF, paired-pulse facilitation; MΩ, megohm; LTD, long term depression; AP, action potential; PP-LFS, paired-pulses low frequency stimulation.

with $Ca_v\beta3$ in the hippocampus (18–20). In addition, N- and L-type VDCCs have been strongly implicated in activity-dependent long lasting synaptic changes, such as LTP, as well as in learning and memory (21, 22). Therefore, we examined the $Ca_v\beta3$-deficient mice (23) for hippocampus-dependent learning and memory and synaptic plasticity. Interestingly, long term memory and NMDAR-dependent LTP were increased in the $Ca_v\beta3$-deficient mice, whereas there was no significant change in Ca^{2+} currents. Furthermore, the mutant mice showed increased NMDAR-mediated synaptic responses and an increased NR2B level in the hippocampus. These results reveal Ca^{2+} channel-independent functions of $Ca_v\beta3$ in the hippocampus.

EXPERIMENTAL PROCEDURES

Animals—The generation of mice lacking $Ca_v\beta3$ was described in our previous study (23). $Ca_v\beta3$ heterozygous ($Ca_v\beta3^{+/-}$) mice were backcrossed into two inbred backgrounds, C57BL/6J and 129S4/SvJae, each over 18 generations. $Ca_v\beta3$ wild-type ($Ca_v\beta3^{+/+}$) and $Ca_v\beta3$-deficient ($Ca_v\beta3^{-/-}$) mice used for analysis were obtained from interbreeding $Ca_v\beta3^{+/-}$ mice of the two backgrounds. Animal care and handling were carried out according to the institutional guidelines. The mice were maintained with free access to food and water under a 12:12-h light/dark cycle. Behavioral experiments were performed on 8–12-week-old mice. All experiments were performed in a blind manner with respect to the genotype.

Contextual and Cued Fear Conditioning—The fear conditioning was carried out as described in our previous study (24). A fear-conditioning shock chamber (19 × 20 × 33 cm) containing a stainless steel rod floor (5 mm diameter, spaced 1 cm apart) and a monitor was used (WinLinc behavioral experimental control software, Coulbourn Instruments). For conditioning, mice were placed in the fear-conditioning apparatus chamber for 2 min, and then a 28-s acoustic conditioned stimulus (CS) was delivered. Following the CS, a 0.5-mA shock of unconditioned stimulus was immediately applied to the floor grid for 2 s. This protocol was performed twice at 60-s interval. To assess contextual learning, the animals were placed back into the training context 24 h after training, and then freezing behavior was observed for 4 min. To assess cued learning, the animals were placed in a different context (a novel chamber, odor, floor, and visual cues) 24 h after training, and their behaviors were monitored for 5 min. During the last 3 min of this test, animals were exposed to the tone. Fear response was quantified by measuring the length of the time when the animal showed freezing behaviors, which was defined as lack of movements with a crouching position, except for respiratory movements (25). Foot-shock intensity was evaluated by placing naive animals in the conditioning chamber used for fear conditioning. Animals were subjected to a 1-s series of gradually increasing mild foot-shock amperage at 20-s intervals as follows: 0.1, 0.15, 0.2, 0.25, 0.3, 0.4, 0.5, and 0.6 mA. The shock intensity that evoked initial sensation responses (flinching and running), vocalization, and jumping was recorded for each mouse.

Novel Object Recognition Memory Task—The task was performed as described (24, 26, 27). The mice were individually habituated to an open-field box (40 × 40 × 40 cm) for 3 days. During the training trial, two objects were placed in the box, and animals were allowed to explore them for 5 min. A mouse was considered to be exploring the object when its head was facing the object within 1-inch distance. Following retention intervals (1 or 24 h), animals were placed back into the box with two objects in the same locations, but one of the familiar objects was replaced by a novel object, and mice were then allowed to explore the two objects for 5 min. The preference percentage, percentage of the time spent exploring the novel object over the total time spent exploring both objects, was used to quantitate the recognition memory.

Social Transmission of Food Preference Task—This task was performed as described previously (21, 28, 29), with slight modifications. "Demonstrator" mice were given a distinctively scented food (cinnamon or cocoa) for 2 h and then immediately allowed to interact with "observer" mice for 30 min. Either 1 or 24 h later, observers were given a choice between two scented foods: either the same scented food that the demonstrators had eaten (cued) or another distinctively scented food (non-cued). Half of the observers in each genotype was subjected to interaction with the demonstrators that had eaten cinnamon as cued food and the other half with those that had eaten cocoa as cued food to control for the possibility of food preference bias.

Whole-cell Patch Clamp Recording on Acutely Isolated CA1 Pyramidal Neurons and on Hippocampal Slices—All experiments were performed on 2–3-week-old mice. Preparation of and recording from hippocampal slices (400 μm thick) were as described in our previous study (21, 30). Hippocampal slices were prepared in oxygenated, cold ACSF (124 mM NaCl, 3.5 mM KCl, 1.25 mM NaH_2PO_4, 2.5 mM $CaCl_2$, 1.3 mM $MgSO_4$, 26 mM $NaHCO_3$, and 10 mM glucose, pH 7.4). For the measurement of Ca^{2+} currents, acutely isolated CA1 pyramidal neurons were prepared from hippocampal slices, as described in our previous study (30). The recorded CA1 neurons were voltage-clamped at −60 mV using glass pipette electrodes (3–5 MΩ series resistance <20 MΩ) and the I-V curve was generated in a stepwise fashion: +10-mV increments from −60 to +40 mV. Internal pipette solution contained the following, 130 mM CsCl, 10 mM EGTA, 10 mM HEPES, 4 mM $MgCl_2$, 4 mM MgATP, 0.3 mM Tris-GTP, 5 mM tetraethylammonium chloride, and was brought to pH 7.4 with NaOH. Extracellular solution contained the following, 25 mM tetraethylammonium chloride, 5 mM 4-aminopyridine, 20 mM HEPES, 3 mM KCl, 5 mM $CaCl_2$, 2 mM $MgCl_2$, 100 mM NaCl, 0.001 mM tetrodotoxin, and was brought to pH 7.4 with NaOH. For the measurement of after hyperpolarization (AHP) currents, visually guided CA1 pyramidal neurons in hippocampal slice were held at −55 mV, and currents were evoked by depolarizing voltage commands to 20 mV for 200 ms followed by a return to −55 mV for 10 s. During recording, the slices were superfused with ACSF at room temperature. Glass pipettes (3–5 MΩ) were filled with solution containing 140 mM $KMeSO_4$, 8 mM NaCl, 1 mM $MgCl_2$, 10 mM HEPES, 2 mM Mg-ATP, 0.4 mM Na_2-GTP, and 0.02 mM EGTA (pH 7.3, 290 mosM). In addition, action potentials (APs) were triggered under current clamp mode by depolarizing current injection (from +30 to +90 pA), and the number of AP (from threshold to the peak) and AP durations (width at half-height) were measured. The internal solution for mEPSC (miniature excitatory

postsynaptic currents) recording was filled with the following buffer, 135 mM potassium gluconate, 5 mM KCl, 2 mM $MgCl_2$, 5 mM EGTA, 10 mM HEPES, 0.5 mM $CaCl_2$, 5 mM Mg-ATP and 0.3 mM Na-GTP, and was brought to pH 7.4 with KOH. The experiment was performed in the presence of tetrodotoxin (1 μM) and bicuculline (10 μM, a GABA type a receptor antagonist). The recorded CA1 pyramidal neurons were voltage-clamped at −70 mV. The frequency and amplitude of mEPSCs were analyzed with MiniAnalysis (Synaptosoft) (21). For the measurement of AMPAR- and NMDAR-mediated synaptic currents in visually guided CA1 pyramidal neurons, pipettes (3–5 MΩ) were filled with the internal solution (130 mM cesium gluconate, 5 mM KCl, 0.1 mM $CaCl_2$, 2.0 mM $MgCl_2$, 5 mM EGTA, 10 mM HEPES, 10 mM QX-314, 4 mM Na-ATP, and 0.4 mM Na-GTP, brought to pH 7.3 with CsOH). The currents were measured in the presence of bicuculline (10 μM) and CGP 55845 (5 μM, a GABA type B receptor antagonist). The synaptic currents were evoked by a bipolar tungsten electrode that was placed in the stratum radiatum. NMDAR- and AMPAR-mediated responses were discriminated based on their distinct kinetics and voltage dependence; the NMDAR-mediated currents were measured at +40 mV, 100 ms after the response onset, whereas the AMPAR-mediated currents were taken as the peak amplitude response recorded at −70 mV (31). D-AP5 (50 μM) blocked the late component of the currents recorded at +40 mV, whereas CNQX (10 μM), an AMPA receptor blocker, eliminated the currents recorded at −70 mV. Whole-cell patch clamp currents were recorded and digitized with a MultiClamp 700A amplifier and a Digidata 1320 or 1322A (Axon Instruments, CA), and acquired data were analyzed with the pCLAMP version 9.2 (Axon Instruments) and the Mini Analysis Program (Synaptosoft).

Extracellular Recording on Hippocampal Slices—Preparation of hippocampal slices and the method of field excitatory postsynaptic potentials (fEPSPs) recording have been described previously (21, 24). Hippocampal slices (400 μm) were prepared from 7–8-week-old mice, as described above. Slices were then placed in a warm, humidified (32 °C, 95% O_2, 5% CO_2) recording chamber containing oxygenated ACSF and maintained for 1.5 h prior to experiments. A bipolar stimulating electrode was placed in the stratum radiatum in the CA1 region, and extracellular field potentials were also recorded in the stratum radiatum using a glass microelectrode (borosilicate glass, 3–5 MΩ, filled with 3 M NaCl). Test responses were elicited at 0.033 Hz. Base-line stimulation was delivered at an intensity that evoked a response that was ~40% of the maximum evoked response. LTP was induced electrically by one of the following protocols: 1) 100-Hz LTP was induced for 100 ms, 300 ms, or 1 s; 2) 200-Hz LTP was induced by 10 trains of 200-ms stimulation at 200 Hz delivered every 5 s. LTD was elicited by paired-pulses low frequency stimulation (PP-LFS) (50-ms pulse interval at 1 Hz for 15 min). Drugs were added to the perfusion medium at least 30 min before recording.

Immunohistology and Western Blot—Immunostaining was performed as described previously (32, 33). Animals were anesthetized and perfused through the heart with 50 ml of cold saline and 50 ml of 4% paraformaldehyde in 0.1 M phosphate buffer. Brains were then removed and were post-fixed overnight. Coronal sections containing hippocampus were stained with the following primary antibodies: anti-β_3 subunit (anti-$Ca_v\beta3$, Alomone Labs), anti-SMI-32, and anti-GAD. A biotinylated secondary antibody and the avidin/biotin system were used for each antibody followed by a 3,3′-diaminobenzidene reaction. Some of the DAB reactions incorporated a nickel intensification procedure. For gross morphology of the hippocampus, Nissl staining was used. For Western blot analysis, total hippocampal proteins were prepared as described previously (34). 25 μg of protein were loaded per lane and analyzed by SDS-PAGE followed by Western blotting. The following antibodies have been described previously: NMDAR 2A/2B (35) and GluR1/2 (34). The following fusion protein was used for the generation of the following polyclonal antibody: H_6-rat NMDAR1 (amino acids 340–561; 1740 guinea pig). Antibody for α-tubulin was purchased from Sigma.

Statistical Analysis—All data are given as mean ± S.E. Two-way repeated ANOVA, one-way ANOVA, and Student's *t* test were used for statistical analyses. $p < 0.05$ was considered statistically significant.

RESULTS

Normal Gross Morphology of the Hippocampus in the $Ca_v\beta3^{-/-}$ Mice—We first examined the cytoarchitectonic divisions in the brain of the $Ca_v\beta3^{-/-}$ mice, especially in the hippocampus. The $Ca_v\beta3^{-/-}$ mice exhibited normal hippocampal divisions, including CA1, CA2, CA3, and dentate gyrus. No expression of $Ca_v\beta3$ was observed in the $Ca_v\beta3^{-/-}$ hippocampus (Fig. 1*A*), whereas $Ca_v\beta3$ was abundant in the wild-type hippocampus as was shown previously (17). The immunoreactivities and the expression patterns of SMI-32 (a neurofilament protein) (Fig. 1*B*) and GAD (GABA-synthesizing enzyme) (Fig. 1*C*) were normally observed in the hippocampus of the $Ca_v\beta3^{-/-}$ mice as in the $Ca_v\beta3^{+/+}$ mice. In addition, Nissl staining of the coronal brain sections revealed no gross abnormalities in the hippocampus of the $Ca_v\beta3^{-/-}$ mice (Fig. 1*D*).

Enhanced Contextual Fear Conditioning in the $Ca_v\beta3^{-/-}$ Mice—Because $Ca_v\beta3$ is highly expressed in the hippocampus and is known to be associated with N- or L-type VDCCs, which play important roles in hippocampus-dependent learning and memory in animals (17–19), we examined whether the deletion of $Ca_v\beta3$ affected the animal's capacity for hippocampus-dependent learning and memory. First, we subjected the mice to the fear conditioning assay that is known to require the function of the hippocampus (36). The $Ca_v\beta3^{+/+}$ ($n = 14$) and $Ca_v\beta3^{-/-}$ ($n = 14$) mice showed similar levels of freezing response during the training (Fig. 2*A*). In the contextual fear memory assay performed 24 h after the training, the $Ca_v\beta3^{-/-}$ mice displayed more freezing behavior than the $Ca_v\beta3^{+/+}$ ($F_{(1, 26)} = 8.36$, $p < 0.01$, two-way repeated ANOVA), indicating an enhanced long term memory of the $Ca_v\beta3^{-/-}$ mice for contextual fear conditioning. A post hoc test (Scheffe's test) also revealed significant differences between the two genotypes during the 2nd ($p < 0.05$), the 3rd ($p < 0.05$), and the 4th min ($p < 0.05$) (Fig. 2*B*). On the other hand, no difference was observed between the two genotypes in the cued fear conditioning assay (Fig. 2*C*), indicating that the enhanced memory in the $Ca_v\beta3^{-/-}$ mice is limited to the hippocampus-dependent fear conditioning. There was no sig-

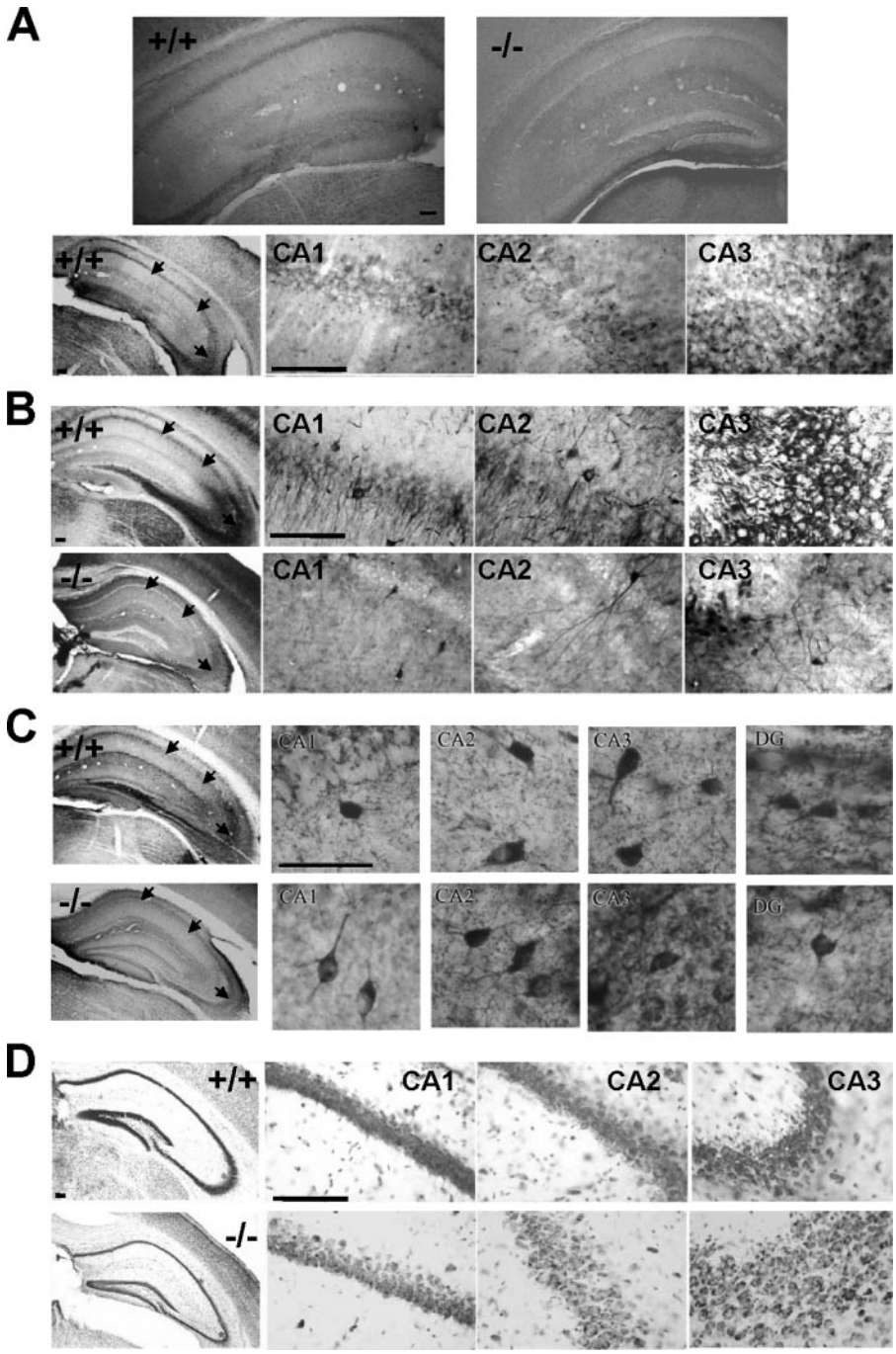

FIGURE 1. **Histological assessment of the hippocampus of the $Ca_v\beta3^{-/-}$ mouse.** *A,* strong immunoreactivity of $Ca_v\beta3$ in the $Ca_v\beta3^{+/+}$ hippocampus indicates that it is highly expressed in the hippocampus, whereas there is no detectable signal in the $Ca_v\beta3^{-/-}$. Similar levels of SMI-32 (*B*) and GAD (*C*) immunoreactivity are observed in the hippocampus of $Ca_v\beta3^{+/+}$ and $Ca_v\beta3^{-/-}$ brain. SMI-32 staining provides Golgi-like staining of neurons/axons, and GAD immunoreactivity is restricted to small interneurons around the pyramidal layer. *D,* normal gross morphology of the hippocampus revealed by Nissl staining in comparable hippocampal regions of $Ca_v\beta3^{+/+}$ and $Ca_v\beta3^{-/-}$ mice. The scale bars equal 100 μm (*A, B,* and *D*) and 50 μm (*C*). *Arrowheads* indicate CA1, CA2, and CA3 region in order.

nificant difference in response to variable electric intensities between $Ca_v\beta3^{-/-}$ ($n = 7$) and $Ca_v\beta3^{+/+}$ ($n = 9$) mice, indicating comparable reactivity or sensitivity to electric foot-shock of the two genotypes (Fig. 2*D*).

Enhanced Novel Object Recognition Memory in the $Ca_v\beta3^{-/-}$ Mice—We next subjected the mice to the novel object recognition task that is based on the animal's ability to discriminate a novel object from a familiar one, which requires the hippocampus (37). We first assessed the amount of time spent by the animals exploring the two objects during the training trial, and we found that both of the genotypes, $Ca_v\beta3^{+/+}$ ($n = 17$) and $Ca_v\beta3^{-/-}$ mice ($n = 14$), explored the two objects for equal time (Fig. 2*E*), which indicated no preference of the animals for either object. At a 1-h retention interval, when one of the familiar objects was replaced by a novel one, both $Ca_v\beta3^{+/+}$ ($n = 8$) and $Ca_v\beta3^{-/-}$ mice ($n = 7$) exhibited increased preference for the novel object to the familiar one ($F_{(1, 13)} = 22.86$, $p < 0.001$, two-way repeated ANOVA). No difference, however, was found between the two genotypes ($F_{(1, 13)} = 0.01$, $p = 0.96$, one-way ANOVA) (+/+, 72.90 ± 4.27%; −/−, 73.34 ± 8.83%) (Fig. 2*F*). At the 24-h retention test, however, $Ca_v\beta3^{-/-}$ mice ($n = 7$) showed increased preference for the novel object compared with $Ca_v\beta3^{+/+}$ ($n = 9$) ($F_{(1, 14)} = 36.14$, $p < 0.001$, two-way repeated ANOVA, Scheffe's post hoc test, $p < 0.01$) (+/+, 62.68 ± 6.26%; −/−, 88.90 ± 3.23%) (Fig. 2*F*), indicating that the $Ca_v\beta3^{-/-}$ mice have an enhanced performance in the object recognition memory task.

Enhanced Long Term Memory in the Social Transmission of Food Preference Task in the $Ca_v\beta3^{-/-}$ Mice—Finally, we carried out the social transmission of food preference assay, another hippocampus-dependent memory task. This task exploits the tendency of mice to prefer food that they have recently smelled on the breath of other mice (demonstrator mice), and subsequently, this tests their ability to learn and remember the information transmitted by olfactory cues during social interactions. 1 h after social interactions with demonstrator mice, both $Ca_v\beta3^{+/+}$ ($n = 7$) and $Ca_v\beta3^{-/-}$ ($n = 6$) mice preferred the "cued" food to the "non-cued" food, and there was no significant difference between the two genotypes (+/+, 83.70 ± 3.63%; −/−, 75.87 ± 7.34%, $F_{(1, 11)} = 0.72$, $p = 0.41$, one-way ANOVA) (Fig. 2*G*). The amount of total food eaten was not different between geno-

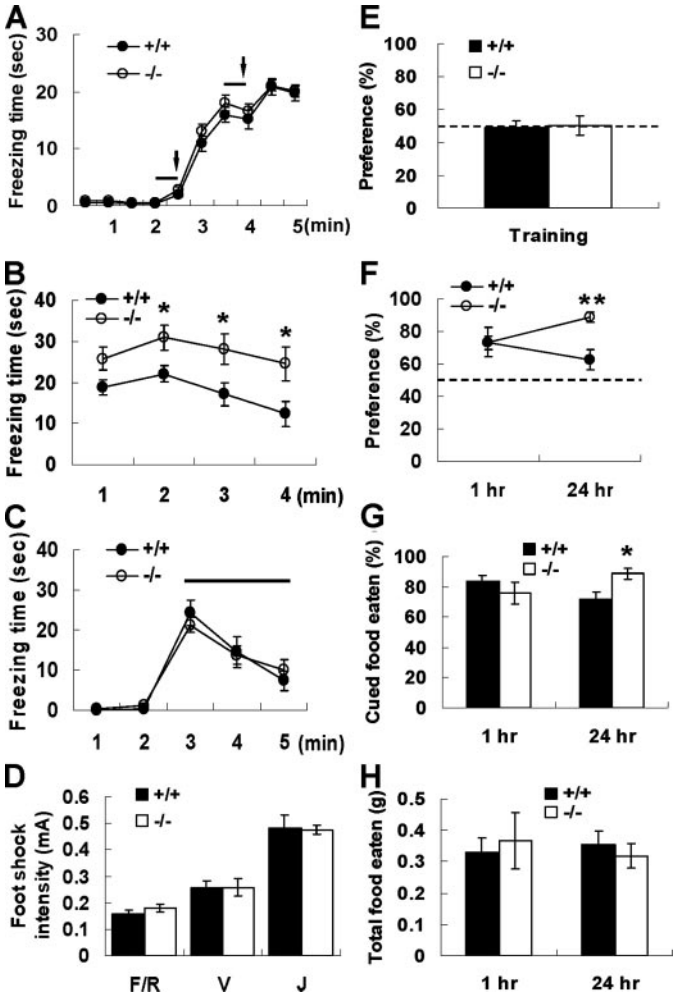

FIGURE 2. **Enhanced long term memory in hippocampus-dependent learning and memory tasks of $Ca_v\beta3^{-/-}$ mice.** *A–D,* fear conditioning. *A,* freezing behavior on the day of training in $Ca_v\beta3^{+/+}$ ($n = 14$) and $Ca_v\beta3^{-/-}$ ($n = 14$). *Solid line* indicates the duration of CS (tone, 28 s), and the *triangles* indicate unconditioned stimulus (foot shock, 2 s). *B,* contextual fear conditioning 24 h after training. $Ca_v\beta3^{-/-}$ mice displayed more freezing behavior than the $Ca_v\beta3^{+/+}$ for contextual fear conditioning. *, $p < 0.05$, Scheffe's post hoc test. *C,* cued fear conditioning 24 h after training. CS (tone) presentation is indicated by the *solid line*. *D,* responses to variable foot shock intensities. *F*, flinching; *R*, running; *V*, vocalization; *J*, jumping. *E* and *F,* novel object recognition task. *E,* mean exploratory preference during training in $Ca_v\beta3^{+/+}$ ($n = 17$) and $Ca_v\beta3^{-/-}$ mice ($n = 14$). *F,* exploration to a novel object after each retention time. At 24 h retention, $Ca_v\beta3^{-/-}$ mice show increased preference for the novel object compared with $Ca_v\beta3^{+/+}$. *Dotted line* indicates equal exploration of all objects. **, $p < 0.01$, Scheffe's post hoc test. *G* and *H,* social transmission of food preference task. *G*, at 1-h retention, both genotypes show a preference for the cued food, and there is no difference between genotypes (+/+, $n = 7$; −/−, $n = 6$). After 24 h, however, $Ca_v\beta3^{-/-}$ mice ($n = 10$) exhibit more preference to cued food than $Ca_v\beta3^{+/+}$ mice ($n = 10$). *, $p < 0.05$, one-way ANOVA. *H,* total food eaten during each test time.

types during this task (Fig. 2*H*). These results indicate that the mice were not deficient in olfaction or social interactions.

On the other hand, 24 h after interactions with demonstrator mice, $Ca_v\beta3^{-/-}$ mice ($n = 10$) exhibited significantly increased preference for cued food compared with $Ca_v\beta3^{+/+}$ mice ($n = 10$) (+/+, 71.61 ± 4.72%; −/−, 88.62 ± 3.56%, $F_{(1, 18)} = 7.10$, $p < 0.05$, one-way ANOVA) (Fig. 2*G*). There was no significant difference between genotypes in the amount of total food that

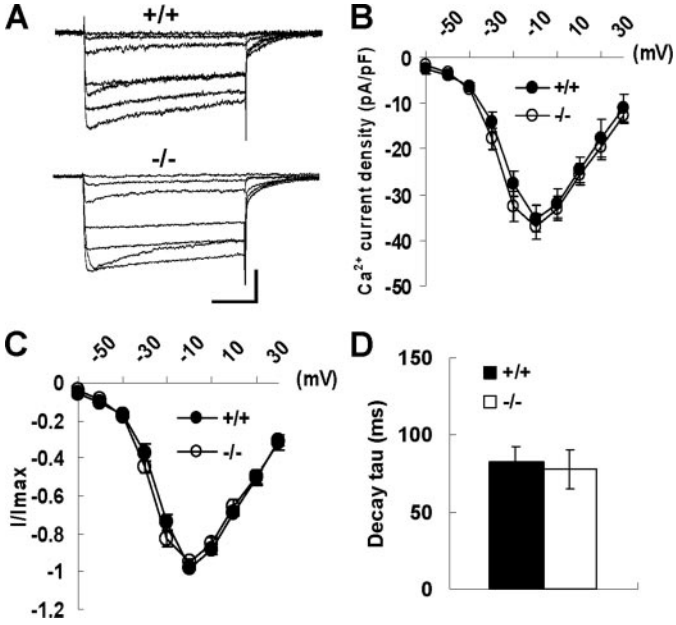

FIGURE 3. **Normal Ca^{2+} currents in hippocampal CA1 pyramidal neurons of $Ca_v\beta3^{-/-}$ mice.** *A,* representative Ca^{2+} current traces in $Ca_v\beta3^{+/+}$ and $Ca_v\beta3^{-/-}$. Ca^{2+} currents were elicited by voltage step depolarizations (+10 mV increments) from −60 mV to +40 mV. *Scale bars*, 200 pA and 50 ms. *B,* I-V curve of total Ca^{2+} currents. There are no differences in total current density between genotypes. The current density was estimated by dividing the peak amplitude by the cell capacitance (pA/pF). *C,* Ca^{2+} current divided by maximum values of Ca^{2+} current (I/I_{max}). *D,* τ value was obtained by fitting current traces evoked at 0 mV to a single exponential curve.

was eaten (Fig. 2*H*). These results suggest that $Ca_v\beta3^{-/-}$ mice displayed an enhanced memory in the social transmission of food preference task.

No Change in Ca^{2+} Currents in the $Ca_v\beta3^{-/-}$ CA1 Pyramidal Neurons—Next we examined whether Ca^{2+} currents (I_{Ca}) are altered or not in the $Ca_v\beta3^{-/-}$ neurons by whole-cell patch clamp recordings in CA1 pyramidal neurons. Total Ca^{2+} currents were activated by step depolarizations (+10-mV increments) from a holding potential of −60 mV (Fig. 3*A*). In CA1 neurons from both $Ca_v\beta3^{+/+}$ and $Ca_v\beta3^{-/-}$ mice, Ca^{2+} currents reached their maximum amplitudes at ~0 mV (Fig. 3*B*). Unlike previous studies that showed a reduced Ca^{2+} current density in $Ca_v\beta3^{-/-}$ neurons (superior cervical ganglion neurons (23), dorsal root ganglion neurons (38), and olfactory sensory neurons (39)), there was no significant difference in the Ca^{2+} current density between $Ca_v\beta3^{+/+}$ and $Ca_v\beta3^{-/-}$ CA1 pyramidal neurons (+/+, 35.46 ± 2.94 pA/pF, $n = 18$, at 0 mV; −/−, 34.80 ± 3.06 pA/pF, $n = 21$, $p = 0.88$, Student's t test) (Fig. 3*B*). Furthermore, there was no difference in the Ca^{2+} current divided by maximum values of the Ca^{2+} current (I/I_{max}) (Fig. 3*C*), and in the time constant (τ) of Ca^{2+} current decay (+/+, 82.70 ± 9.75 ms; −/−, 77.70 ± 12.58 ms, $p = 0.76$, Student's t test) (Fig. 3*D*), indicating no changes in voltage dependence and inactivating kinetics in the $Ca_v\beta3^{-/-}$ CA1 neurons.

Normal Intrinsic Firing Properties and AHP Currents in the $Ca_v\beta3^{-/-}$—As a close coupling was reported by co-immunoprecipitation between $Ca_v\beta3$ and N- or L-type VDCCs in hippocampal neurons (18–20), we measured N- or L-type VDCCs-mediated cellular properties in CA1 neurons. Ca^{2+} influx

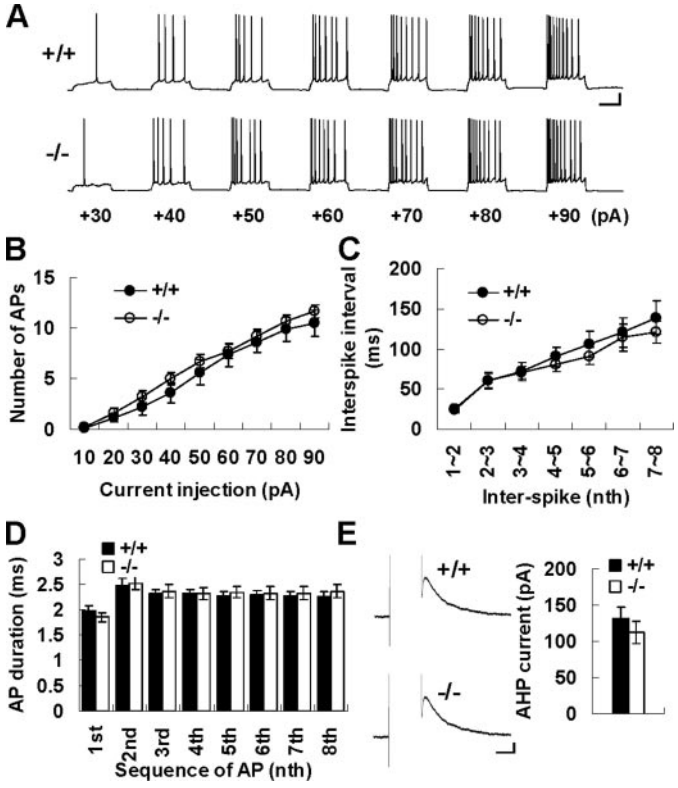

FIGURE 4. **Normal firing properties and normal AHP currents of $Ca_v\beta3^{-/-}$ CA1 pyramidal neurons.** *A,* action potentials are generated by increasing depolarizing current injections from +30 to 90 pA. *Scale bars,* 15 mV and 500 ms. *B,* number of APs evoked at different current injections. *C* and *D,* there are no significant differences in the interspike intervals (*C*) and the duration (half-width) (*D*) of APs between genotypes during a 90-pA current injection. *E,* voltage clamp recordings of AHP current after a 200-ms depolarization pulse to +20 mV. *Bar graph* indicates the amplitudes of AHP current measured at 30 ms after pulse-offset. *Scale bars,* 40 pA and 100 ms.

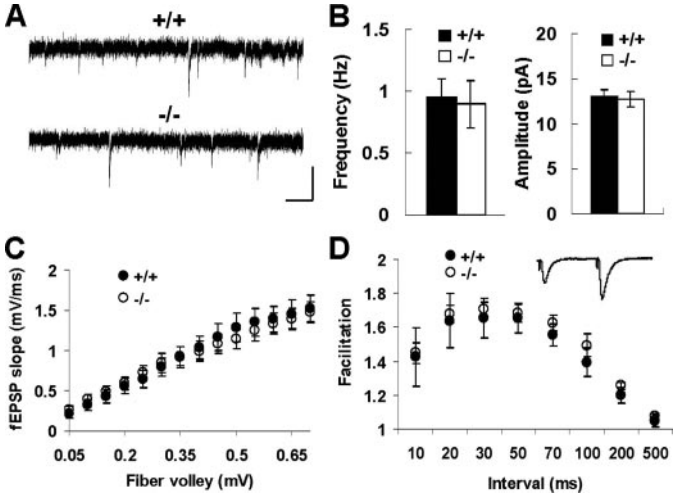

FIGURE 5. **Basal synaptic functions at hippocampal CA3-CA1 synapses in the $Ca_v\beta3^{-/-}$.** *A,* representative sample traces of mEPSCs from $Ca_v\beta3^{+/+}$ and $Ca_v\beta3^{-/-}$ mice. *Scale bars,* 20 pA and 500 ms. *B,* frequencies (*left*) and amplitudes (*right*) of mEPSCs in CA1 pyramidal neurons were not statistically different between the two genotypes. *C,* slope of fEPSPs elicited by a given presynaptic fiber volley. The input-output relationship of basal synaptic transmission is not altered in $Ca_v\beta3^{-/-}$ mice. *D,* normal PPF in the $Ca_v\beta3^{-/-}$. Traces are responses at 50-ms interpulse interval.

through N- or L-type VDCCs is known to be linked to the functions of Ca^{2+}-activated K^+ channels that are involved in shaping of APs, including the duration of AP and after hyperpolarization (AHP), and thus can modulate firing properties (40). First we produced AP discharges by a depolarizing current injection under the current clamp mode (Fig. 4*A*). The CA1 pyramidal neurons of $Ca_v\beta3^{+/+}$ ($n = 8$) and $Ca_v\beta3^{-/-}$ ($n = 13$) displayed very similar firing patterns. No significant difference was observed in the interspike intervals (Fig. 4*C*), the number (Fig. 4*B*) and duration (Fig. 4*D*) of APs. To directly assess the functions of Ca^{2+}-activated K^+ channels, we recorded AHP currents. Again, there was no difference in the AHP current between the $Ca_v\beta3^{+/+}$ ($n = 8$) and the $Ca_v\beta3^{-/-}$ ($n = 9$) (+/+, 131.60 ± 15.86 pA; −/−, 112.16 ± 15.42 pA, $p = 0.41$, Student's *t* test) (Fig. 4*E*). These results show that the $Ca_v\beta3^{-/-}$ mutation did not affect intrinsic firing behaviors of hippocampal CA1 neurons.

Normal Basal Synaptic Transmission and Short Term Plasticity in the $Ca_v\beta3^{-/-}$ Mice—We then examined the basal synaptic function at hippocampal CA3-CA1 synapses in the $Ca_v\beta3^{-/-}$ mice. In mEPSCs (Fig. 5*A*), $Ca_v\beta3^{-/-}$ mice showed frequencies and amplitudes similar to those of $Ca_v\beta3^{+/+}$ mice (Fig. 5*B*). In addition, fEPSPs were recorded from the CA1 area of the hippocampus in response to stimulations of Schaffer collateral fibers. As illustrated in Fig. 5*C*, the input-output relation of synaptic transmission was not altered in the $Ca_v\beta3^{-/-}$ mice (+/+, $n = 10$; −/−, $n = 12$). We next studied the effect of the $Ca_v\beta3$ mutation on paired-pulse facilitation (PPF), a presynaptic form of short term plasticity. PPF is a transient enhancement of neurotransmitter release induced by two closely spaced stimuli. This increase in release is usually attributed to intracellular Ca^{2+} concentration in the presynaptic terminal following the first stimulus (41, 42). There were no significant differences in all tested interpulse intervals between the $Ca_v\beta3^{+/+}$ ($n = 7$) and the $Ca_v\beta3^{-/-}$ ($n = 9$) (Fig. 5*D*). Taken together, these results indicate that the $Ca_v\beta3$ mutation had no significant effect upon the basal synaptic function and the presynaptic short term plasticity in hippocampal CA3-CA1 synapses.

Enhanced NMDAR-dependent LTP in the $Ca_v\beta3^{-/-}$ Mice—We then investigated the mutant mice for activity-dependent long lasting synaptic changes, such as LTP and LTD, a cellular model of learning and memory (43). We tried to induce LTP by several different stimulation protocols. LTP was induced by 100-Hz (300 ms and 1 s) or 200-Hz tetanic stimulations. As shown in Fig. 6*A*, an administration of tetanus at 100 Hz for 1 s elicited a significantly increased potentiation in the $Ca_v\beta3^{-/-}$ compared with that in the $Ca_v\beta3^{+/+}$ (−/−, 169.47 ± 7.33% of base line at 60 min, $n = 9$; +/+, 144.75 ± 6.10%, $n = 9$, $p < 0.05$, Student's *t* test). With a 200-Hz tetanic stimulation, the $Ca_v\beta3^{-/-}$ also exhibited more robust potentiation than $Ca_v\beta3^{+/+}$ (−/−, 231.92 ± 15.72% of base line at 60 min, $n = 10$; +/+, 181.74 ± 17.58%, $n = 8$, $p < 0.05$, Student's *t* test) (Fig. 6*B*). Even at short 100-Hz stimulations for 300 ms, enhanced LTP in the $Ca_v\beta3^{-/-}$ was also observed (−/−, 139.31 ± 7.35% of base line at 60 min, $n = 10$; +/+, 114.70 ± 8.03%, $n = 8$, $p < 0.05$, Student's *t* test) (Fig. 6*C*). However, in the presence of D-AP5, a specific NMDAR inhibitor, the enhancement of LTP in the $Ca_v\beta3^{-/-}$ disappeared under the same stimulation condition, and a similar level of potentiation was induced in the two genotypes (Fig. 6, *D* and *E*). Together, these results indicate that

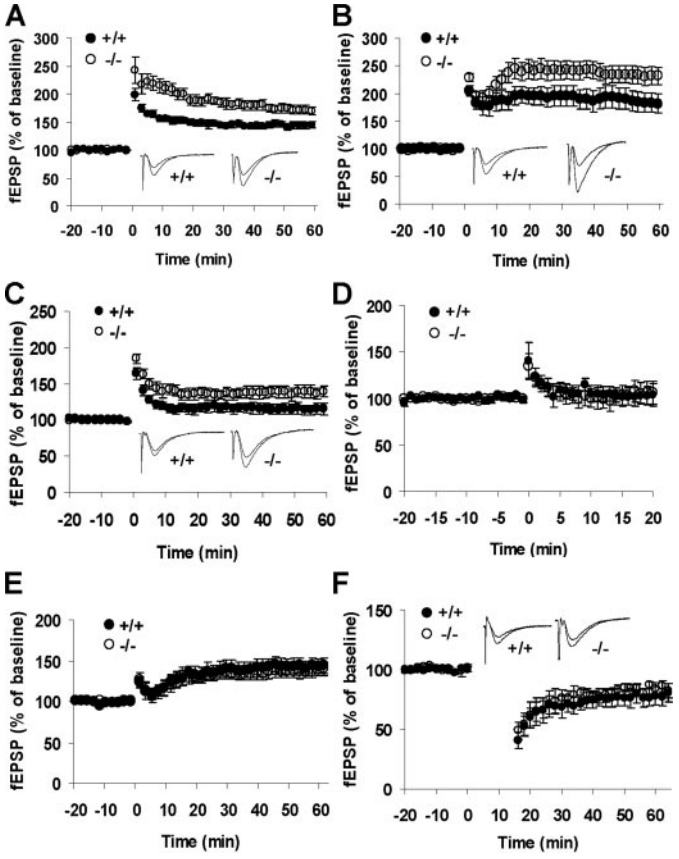

FIGURE 6. **Enhanced LTP in the $Ca_v\beta3^{-/-}$.** *A,* LTP elicited by tetanus at 100 Hz for 1 s. LTP of $Ca_v\beta3^{-/-}$ is significantly higher than that of $Ca_v\beta3^{+/+}$ mice ($p < 0.05$). *B,* LTP elicited by stimulations at 200 Hz. $Ca_v\beta3^{-/-}$ mice also showed enhanced LTP ($p < 0.05$). *C,* LTP elicited by tetanus at 100 Hz for 300 ms. LTP of $Ca_v\beta3^{-/-}$ is significantly higher than that of $Ca_v\beta3^{+/+}$ mice ($p < 0.05$). *D* and *E,* in the presence of D-AP5 (50 μM), LTP elicited by stimulations at 100 Hz (*D*) 200 Hz (*E*). There is no significant difference between genotypes. *F,* LTD was induced by PP-LFS.

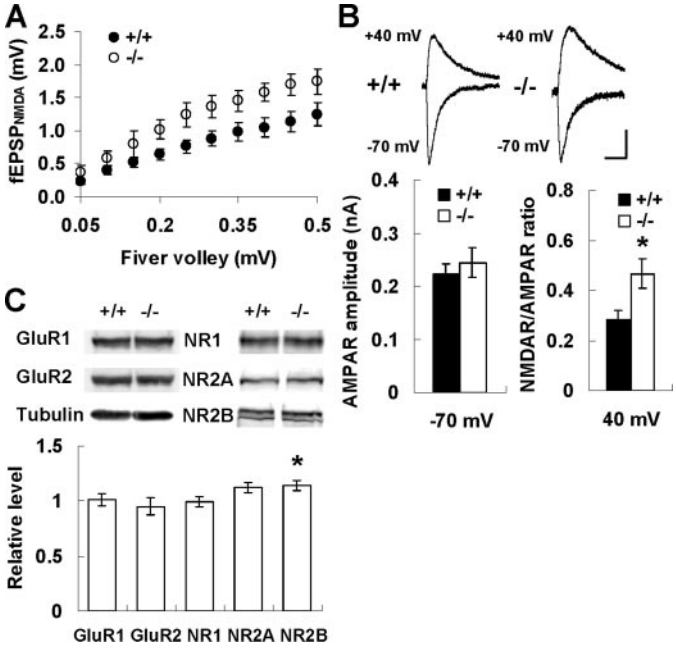

FIGURE 7. **Increased NMDAR-mediated responses and increased NR2B levels in the hippocampus of $Ca_v\beta3^{-/-}$ mice.** *A,* NMDAR-mediated synaptic potentials in the presence of CNQX (10 μM) and reduced Mg^{2+} (0.1 mM). The $Ca_v\beta3^{-/-}$ shows higher NMDAR-mediated fEPSPs than $Ca_v\beta3^{+/+}$ ($F_{(1, 23)} = 5.52$, $p < 0.05$, two-way repeated ANOVA). *B,* NMDAR- and AMPAR-mediated EPSCs recorded under voltage clamp. Representative traces of EPSCs evoked at −70 mV and +40 mV in $Ca_v\beta3^{+/+}$ and $Ca_v\beta3^{-/-}$. *Scale bars,* 0.1 nA and 50 ms. There are no differences in AMPAR-mediated EPSCs at −70 mV between genotypes (*left bar graph*), but the ratio of NMDAR/AMPAR response in the $Ca_v\beta3^{-/-}$ is higher than that of the $Ca_v\beta3^{+/+}$ (*right bar graph*). NMDAR-mediated responses were taken from the amplitude of currents at +40 mV, 100 ms after EPSCs onset, whereas the AMPAR-mediated responses were taken as the peak amplitude of EPSCs recorded at −70 mV. *, $p < 0.05$. *C,* Western blot analysis. The relative levels of glutamate receptors in hippocampal proteins of $Ca_v\beta3^{-/-}$ mice. The NR2B level of $Ca_v\beta3^{-/-}$ mice was relatively increased, whereas other glutamate receptors did not change. The equal amount of protein loading was confirmed by normalizing against the amount of tubulin. *, $p < 0.05$.

the increased potentiation in the $Ca_v\beta3^{-/-}$ is NMDAR-dependent LTP. No significant difference was noted between the two genotypes in LTD that was induced by PP-LFS (Fig. 6*F*).

Increased NMDAR-mediated Synaptic Currents and NR2B Levels in the $Ca_v\beta3^{-/-}$ Mice—NMDAR is known to play a crucial role in LTP, as well as learning and memory (43–46). Therefore, we examined the possibility that changes in the synaptic responses mediated by NMDAR might underlie the increased LTP in $Ca_v\beta3^{-/-}$ mice. To evaluate this possibility, we first measured the NMDAR-mediated fEPSPs by adding CNQX (10 μM), an AMPA receptor blocker, to the buffer with reduced Mg^{2+} concentration (0.1 mM). A significant difference was noted between the $Ca_v\beta3^{+/+}$ and the $Ca_v\beta3^{-/-}$ in these NMDAR-mediated field responses; the $Ca_v\beta3^{-/-}$ ($n = 13$) exhibited higher NMDAR-mediated fEPSPs than the $Ca_v\beta3^{+/+}$ ($n = 12$) ($F_{(1, 23)} = 5.52$, $p < 0.05$, two-way repeated ANOVA) (Fig. 7*A*). To assess this finding more directly, we measured the excitatory postsynaptic currents (EPSCs) evoked by stimulations at Schaffer collateral axons under the whole-cell voltage clamp conditions in CA1 neurons. It was found that there was no significant difference in the amplitude of AMPAR-mediated EPSCs at −70 mV between the two genotypes (Fig. 7*B*, *left*). However, a significant difference was noted in the NMDAR/AMPAR amplitude ratio between $Ca_v\beta3^{+/+}$ ($n = 15$, 0.28 ± 0.04 at +40 mV) and $Ca_v\beta3^{-/-}$ ($n = 13$, 0.47 ± 0.06 at +40 mV) ($p < 0.05$, Student *t* test) (Fig. 7*B*, *right*). Together, these results indicate that NMDAR-mediated responses are increased in $Ca_v\beta3^{-/-}$ mice.

In an effort to obtain some clue for the mechanism underlying the increased NMDAR responses in the $Ca_v\beta3^{-/-}$ mice, we quantified the levels of NMDAR subunits by Western blot analysis. It was found that the protein level of NR2B subunit in the hippocampus of the $Ca_v\beta3^{-/-}$ mice ($n = 3$, 1.14 ± 0.05, normalized to $Ca_v\beta3^{+/+}$ values) was slightly increased relative to that of the $Ca_v\beta3^{+/+}$ mice ($n = 3$) ($p < 0.05$, Student's *t* test) (Fig. 7*C*). There were no significant changes in the levels of other glutamate receptors.

DISCUSSION

In this study, we analyzed the $Ca_v\beta3$-deficient mice with respect to their capacity for learning/memory and synaptic plasticity. Although there was no change in VDCCs currents and basal synaptic transmission, we found that the deletion of $Ca_v\beta3$ caused an increase of NR2B expression and NMDAR activities, including currents and LTP, in the hippocampus and an enhanced capacity for learning and memory. This study

demonstrates a previously unidentified outcome of the deletion of $Ca_v\beta3$ in the adult brain.

Yet the $Ca_v\beta$ subunits of VDCCs have been known to be associated with VDCCs and regulate Ca^{2+} influx through VDCCs by modulating the properties of VDCCs α_1 subunits, including trafficking of channel complexes to the plasma membrane, Ca^{2+} current densities, and voltage-dependent activation or inactivation (4, 5). Of the $Ca_v\beta$ subtypes, the $Ca_v\beta3$ is the predominant form in the brain (17), and its role in several neurons has been revealed by studies carried out using mice lacking the $Ca_v\beta3$. In superior cervical ganglion neurons, the $Ca_v\beta3^{-/-}$ showed reduced N- and L-type Ca^{2+} currents relative to the $Ca_v\beta3^{+/+}$ and shifting of voltage-dependent activation in P/Q-type Ca^{2+} currents (23). In dorsal root ganglion neurons, the $Ca_v\beta3^{-/-}$ mice showed a reduced expression of N-type VDCCs and functional alterations of Ca^{2+} currents, which was thought to be involved in the reduced pain responses of the $Ca_v\beta3^{-/-}$ mice (38). In olfactory sensory neurons, the $Ca_v\beta3^{-/-}$ mice also exhibited decreased protein expressions and Ca^{2+} currents of L-type and N-type VDCCs, leading to increased olfactory neuronal activities (39). These reduced expressions of proteins or Ca^{2+} currents of VDCCs might be considered to mostly result from deficiency in trafficking of channel complexes to the plasma membrane.

However, although the $Ca_v\beta3$ is known to be highly expressed in the hippocampus (17) and has been shown to associate with 42% of the α_1 subunits of L-type VDCCs in the hippocampus (18), we could not observe a change in nifedipine-sensitive L-type Ca^{2+} currents in hippocampal CA1 pyramidal neurons of the $Ca_v\beta3^{-/-}$ mice (supplemental Fig. 1). In addition, there were no clear differences in the patterns of the immunohistological labeling for the α1C ($Ca_v1.2$) and the α1D ($Ca_v1.3$) subunits of L-type VDCCs in the hippocampus, between the two genotypes (supplemental Fig. 2). Furthermore, although $Ca_v\beta3$ in the brain was shown to associate with about 52% α1B subunit of N-type VDCCs that play a crucial role in neurotransmitter release at hippocampal CA3-CA1 synapses (19–21, 47, 48), the basal synaptic transmission, including mEPSCs, was not altered at hippocampal CA3-CA1 synapses of the $Ca_v\beta3^{-/-}$ mice. Therefore, some compensation by other $Ca_v\beta$ isotypes might have occurred for the deletion of $Ca_v\beta3$ in the hippocampus of the $Ca_v\beta3^{-/-}$ mice, as was reported in olfactory sensory neurons of the $Ca_v\beta3^{-/-}$ mice (39).

Instead, however, we found an increased LTP at hippocampal CA3-CA1 synapses in the $Ca_v\beta3^{-/-}$ mice. The induction of LTP by a tetanic stimulation at 100 Hz is known to be dependent on NMDAR, and 200-Hz LTP requires both NMDAR and L-type VDCCs at hippocampal CA3-CA1 synapses (49). When NMDAR was blocked by D-AP5, the enhancement in 100-Hz and 200-Hz LTP of the $Ca_v\beta3^{-/-}$ mice was obliterated. This indicates that the increased potentiation in the $Ca_v\beta3^{-/-}$ is of the NMDAR-dependent component in LTP, rather than L-type VDCC-dependent. The increased LTP and long term memory in the $Ca_v\beta3^{-/-}$ mice could be analogous to other cases where an alteration of NMDAR-mediated synaptic responses resulting from the increased levels of NR2B was shown (45, 46).

Although the Ca^{2+} currents and mEPSCs were measured from 2- to 3-week-old mice, basal synaptic transmission and LTP were recorded in 7- to 8-week-old mice. Thus, no alteration in Ca^{2+} currents of at least N- and L-type VDCCs could be expected in the adult $Ca_v\beta3^{-/-}$ mice, because they showed normal responses in basal synaptic transmission and NMDA-independent LTP, in which N- and L-type VDCCs have a crucial role, respectively (21, 22, 47–49).

Our results suggest a possibility that $Ca_v\beta3$ can be a multifunctional protein as was shown for other $Ca_v\beta$ isotypes. The studies of crystal structures revealed that $Ca_v\beta$ subunits belong to membrane-associated guanylate kinase family that has scaffolding functions, suggesting that the $Ca_v\beta$ can play a role in scaffolding multiple signaling pathways by protein-protein interactions through SH3 and GK domains (6, 8, 9). Recently, it was suggested that the $Ca_v\beta$ could directly interact with other proteins, and furthermore it could function without marked influences on the property of VDCCs (10, 11, 50). The physiological unbinding of the $Ca_v\beta$ from the VDCCs complex has already been demonstrated from the inactivation heterogeneity of VDCCs and reversibility of the interaction with α_1 subunits (51, 52). It was reported that $Ca_v\beta$ could directly bind to Gem and Rem, small G-proteins that have a GTPase activity, and this interaction inhibited the surface expression and the activity of VDCCs (12, 13). In addition, it was also shown that $Ca_v\beta$ could promote endocytosis of VDCCs by interaction with dynamin (14). A short splice variant of $Ca_v\beta4$ could directly interact with CHCB2, a nuclear protein, and then translocate into the nucleus for the subsequent regulation of gene transcription in the cochlea (15). In this study, it was found that the $Ca_v\beta$ could function independently from VDCCs without marked influences on the surface expression and voltage-dependent properties of VDCCs. Furthermore, inositol 1,4,5-trisphosphate-mediated signaling was enhanced in $Ca_v\beta3$-deficient pancreatic β cells, whereas Ca^{2+} currents of VDCCs were not affected (16). Similarly, $Ca_v\beta$ were found to internalize Shaker K^+ channels by association with dynamin (14). These activities of $Ca_v\beta$ are considered to be completely independent of VDCCs regulation, and thus indicate that $Ca_v\beta$ can function as a multifunctional protein by interactions with other proteins. In this light, it might be possible that the $Ca_v\beta3$ can directly or indirectly associate with NR2B.

Although our results showed a modest increase of NR2B in the mutant, it is not clear whether this increase can totally explain how the NMDAR activities are enhanced. In the meantime, it was discovered that the C-terminal tail region of $Ca_v1.3$ L-type VDCC bound to the SH3 domain of Shank, a postsynaptic scaffolding protein (53–55). Shank is also known to associate with GKAP-PSD95-NR2B through postsynaptic density-95 (PSD-95)/Discs large/zona occludens-1 domain (56). One of the binding sites of $Ca_v\beta$ is the C-terminal tail region of α_1 subunits of VDCCs (6, 8, 9, 57). In this light, the removal of $Ca_v\beta3$ might have an influence on the interaction of VDCCs and their partners and then could lead to an alteration in the NMDAR activity. Alternatively, we cannot rule out the possibility that a compensatory increase of other $Ca_v\beta$ isotypes or other developmental compensation, which may have occurred in the $Ca_v\beta3^{-/-}$ hippocampus, could also be linked to the alteration in the NMDAR activity. In addition, previously described behavioral alterations from the changes in dorsal root ganglion

or olfactory neuronal activities in the $Ca_v\beta3^{-/-}$ mice (38, 39) could contribute to the phenotypes shown in our results.

Initially, we started investigating the role of the $Ca_v\beta3$ in synaptic transmission and hippocampus-dependent learning and memory because of its known relationship with N- or L-type VDCCs. Interestingly, we found that the ablation of $Ca_v\beta3$ led to enhanced LTP and capacity for learning and memory in the animal. These phenotypes appear to be due to the increased NMDAR activity with increased NR2B levels in the $Ca_v\beta3^{-/-}$ mice. Even though the precise mechanism of the enhancement of the NMDAR activity in the $Ca_v\beta3^{-/-}$ mice is not yet completely understood, our experiments may reveal a potentially novel function of $Ca_v\beta3$, unrelated to a role associated with VDCCs. Further studies of the relationship, including direct or indirect protein-protein interactions, between $Ca_v\beta3$ and NMDAR will be needed to confirm this role of $Ca_v\beta3$ in the adult brain.

Acknowledgments—We thank Dr. Minjeong Sun, Seungeun Lee, and Sangwoo Kim for help in behavioral experiments and Jeremy Mills and Erick Green for help with histology.

REFERENCES

1. Hofmann, F., Lacinova, L., and Klugbauer, N. (1999) *Rev. Physiol. Biochem. Pharmacol.* **139,** 33–87
2. Catterall, W. A. (2000) *Neuron* **26,** 13–25
3. Ertel, E. A., Campbell, K. P., Harpold, M. M., Hofmann, F., Mori, Y., Perez-Reyes, E., Schwartz, A., Snutch, T. P., Tanabe, T., Birnbaumer, L., Tsien, R. W., and Catterall, W. A. (2000) *Neuron* **25,** 533–535
4. Berrow, N. S., Campbell, V., Fitzgerald, E. M., Brickley, K., and Dolphin, A. C. (1995) *J. Physiol.* (*Lond.*) **482,** 481–491
5. Dolphin, A. C. (2003) *J. Bioenerg. Biomembr.* **35,** 599–620
6. Chen, Y. H., Li, M. H., Zhang, Y., He, L. L., Yamada, Y., Fitzmaurice, A., Shen, Y., Zhang, H., Tong, L., and Yang, J. (2004) *Nature* **429,** 675–680
7. Hanlon, M. R., Berrow, N. S., Dolphin, A. C., and Wallace, B. A. (1999) *FEBS Lett.* **445,** 366–370
8. Opatowsky, Y., Chen, C. C., Campbell, K. P., and Hirsch, J. A. (2004) *Neuron* **42,** 387–399
9. Van Petegem, F., Clark, K. A., Chatelain, F. C., and Minor, D. L., Jr. (2004) *Nature* **429,** 671–675
10. Hidalgo, P., and Neely, A. (2007) *Cell Calcium* **42,** 389–396
11. Rousset, M., Cens, T., and Charnet, P. (2005) *Sci. STKE 2005,* PE11
12. Beguin, P., Nagashima, K., Gonoi, T., Shibasaki, T., Takahashi, K., Kashima, Y., Ozaki, N., Geering, K., Iwanaga, T., and Seino, S. (2001) *Nature* **411,** 701–706
13. Finlin, B. S., Crump, S. M., Satin, J., and Andres, D. A. (2003) *Proc. Natl. Acad. Sci. U. S. A.* **100,** 14469–14474
14. Gonzalez-Gutierrez, G., Miranda-Laferte, E., Neely, A., and Hidalgo, P. (2007) *J. Biol. Chem.* **282,** 2156–2162
15. Hibino, H., Pironkova, R., Onwumere, O., Rousset, M., Charnet, P., Hudspeth, A. J., and Lesage, F. (2003) *Proc. Natl. Acad. Sci. U. S. A.* **100,** 307–312
16. Berggren, P. O., Yang, S. N., Murakami, M., Efanov, A. M., Uhles, S., Kohler, M., Moede, T., Fernstrom, A., Appelskog, I. B., Aspinwall, C. A., Zaitsev, S. V., Larsson, O., de Vargas, L. M., Fecher-Trost, C., Weissgerber, P., Ludwig, A., Leibiger, B., Juntti-Berggren, L., Barker, C. J., Gromada, J., Freichel, M., Leibiger, I. B., and Flockerzi, V. (2004) *Cell* **119,** 273–284
17. Ludwig, A., Flockerzi, V., and Hofmann, F. (1997) *J. Neurosci.* **17,** 1339–1349
18. Pichler, M., Cassidy, T. N., Reimer, D., Haase, H., Kraus, R., Ostler, D., and Striessnig, J. (1997) *J. Biol. Chem.* **272,** 13877–13882
19. Scott, V. E., De Waard, M., Liu, H., Gurnett, C. A., Venzke, D. P., Lennon, V. A., and Campbell, K. P. (1996) *J. Biol. Chem.* **271,** 3207–3212
20. Vance, C. L., Begg, C. M., Lee, W. L., Haase, H., Copeland, T. D., and McEnery, M. W. (1998) *J. Biol. Chem.* **273,** 14495–14502
21. Jeon, D., Kim, C., Yang, Y. M., Rhim, H., Yim, E., Oh, U., and Shin, H. S. (2007) *Genes Brain Behav.* **6,** 375–388
22. Moosmang, S., Haider, N., Klugbauer, N., Adelsberger, H., Langwieser, N., Muller, J., Stiess, M., Marais, E., Schulla, V., Lacinova, L., Goebbels, S., Nave, K. A., Storm, D. R., Hofmann, F., and Kleppisch, T. (2005) *J. Neurosci.* **25,** 9883–9892
23. Namkung, Y., Smith, S. M., Lee, S. B., Skrypnyk, N. V., Kim, H. L., Chin, H., Scheller, R. H., Tsien, R. W., and Shin, H. S. (1998) *Proc. Natl. Acad. Sci. U. S. A.* **95,** 12010–12015
24. Jeon, D., Yang, Y. M., Jeong, M. J., Philipson, K. D., Rhim, H., and Shin, H. S. (2003) *Neuron* **38,** 965–976
25. Lu, Y. M., Jia, Z., Janus, C., Henderson, J. T., Gerlai, R., Wojtowicz, J. M., and Roder, J. C. (1997) *J. Neurosci.* **17,** 5196–5205
26. Mansuy, I. M., Winder, D. G., Moallem, T. M., Osman, M., Mayford, M., Hawkins, R. D., and Kandel, E. R. (1998) *Neuron* **21,** 257–265
27. Podhorna, J., and Brown, R. E. (2002) *Genes Brain Behav.* **1,** 96–110
28. Bunsey, M., and Eichenbaum, H. (1995) *Hippocampus* **5,** 546–556
29. Kogan, J. H., Frankland, P. W., Blendy, J. A., Coblentz, J., Marowitz, Z., Schutz, G., and Silva, A. J. (1997) *Curr. Biol.* **7,** 1–11
30. Song, I., Kim, D., Choi, S., Sun, M., Kim, Y., and Shin, H. S. (2004) *J. Neurosci.* **24,** 5249–5257
31. Saura, C. A., Choi, S. Y., Beglopoulos, V., Malkani, S., Zhang, D., Shankaranarayana Rao, B. S., Chattarji, S., Kelleher, R. J., III, Kandel, E. R., Duff, K., Kirkwood, A., and Shen, J. (2004) *Neuron* **42,** 23–36
32. Jeon, D., Chu, K., Jung, K. H., Kim, M., Yoon, B. W., Lee, C. J., Oh, U., and Shin, H. S. (2007) *Cell Calcium,* in press
33. Kang, Y. S., Kong, J. H., Park, W. M., Kwon, O. J., Lee, J. E., Kim, S. Y., and Jeon, C. J. (2002) *Mol. Cells* **14,** 361–366
34. Elias, G. M., Funke, L., Stein, V., Grant, S. G., Bredt, D. S., and Nicoll, R. A. (2006) *Neuron* **52,** 307–320
35. Sheng, M., Cummings, J., Roldan, L. A., Jan, Y. N., and Jan, L. Y. (1994) *Nature* **368,** 144–147
36. Phillips, R. G., and LeDoux, J. E. (1992) *Behav. Neurosci.* **106,** 274–285
37. Vnek, N., and Rothblat, L. A. (1996) *J. Neurosci.* **16,** 2780–2787
38. Murakami, M., Fleischmann, B., De Felipe, C., Freichel, M., Trost, C., Ludwig, A., Wissenbach, U., Schwegler, H., Hofmann, F., Hescheler, J., Flockerzi, V., and Cavalie, A. (2002) *J. Biol. Chem.* **277,** 40342–40351
39. Shiraiwa, T., Kashiwayanagi, M., Iijima, T., and Murakami, M. (2007) *Biochem. Biophys. Res. Commun.* **355,** 1019–1024
40. Faber, E. S., and Sah, P. (2003) *Neuroscientist* **9,** 181–194
41. Regehr, W. G., Delaney, K. R., and Tank, D. W. (1994) *J. Neurosci.* **14,** 523–537
42. Zucker, R. S. (1999) *Curr. Opin. Neurobiol.* **9,** 305–313
43. Bliss, T. V., and Collingridge, G. L. (1993) *Nature* **361,** 31–39
44. McGaugh, J. L. (2000) *Science* **287,** 248–251
45. Tang, Y. P., Shimizu, E., Dube, G. R., Rampon, C., Kerchner, G. A., Zhuo, M., Liu, G., and Tsien, J. Z. (1999) *Nature* **401,** 63–69
46. Tsien, J. Z., Huerta, P. T., and Tonegawa, S. (1996) *Cell* **87,** 1327–1338
47. Dunlap, K., Luebke, J. I., and Turner, T. J. (1995) *Trends Neurosci.* **18,** 89–98
48. Wu, L. G., and Saggau, P. (1997) *Trends Neurosci.* **20,** 204–212
49. Cavus, I., and Teyler, T. (1996) *J. Neurophysiol.* **76,** 3038–3047
50. Dolphin, A. C. (2006) *Br. J. Pharmacol.* **147,** S56–S62
51. Bichet, D., Lecomte, C., Sabatier, J. M., Felix, R., and De Waard, M. (2000) *Biochem. Biophys. Res. Commun.* **277,** 729–735
52. Restituito, S., Cens, T., Rousset, M., and Charnet, P. (2001) *Biophys. J.* **81,** 89–96
53. Olson, P. A., Tkatch, T., Hernandez-Lopez, S., Ulrich, S., Ilijic, E., Mugnaini, E., Zhang, H., Bezprozvanny, I., and Surmeier, D. J. (2005) *J. Neurosci.* **25,** 1050–1062
54. Sheng, M., and Kim, E. (2000) *J. Cell Sci.* **113,** 1851–1856
55. Zhang, H., Maximov, A., Fu, Y., Xu, F., Tang, T. S., Tkatch, T., Surmeier, D. J., and Bezprozvanny, I. (2005) *J. Neurosci.* **25,** 1037–1049
56. Naisbitt, S., Kim, E., Tu, J. C., Xiao, B., Sala, C., Valtschanoff, J., Weinberg, R. J., Worley, P. F., and Sheng, M. (1999) *Neuron* **23,** 569–582
57. Walker, D., and De Waard, M. (1998) *Trends Neurosci.* **21,** 148–154